



# A finite element method enriched for wave propagation problems

Seounghyun Ham, Klaus-Jürgen Bathe\*

Massachusetts Institute of Technology, Cambridge, MA 02139, United States

## ARTICLE INFO

### Article history:

Received 12 October 2011

Accepted 1 January 2012

Available online 26 January 2012

### Keywords:

Wave propagation

Finite elements

Spectral methods

Harmonics

Enriched finite elements

Implicit time integration

## ABSTRACT

An enriched finite element method is presented to solve various wave propagation problems. The proposed method is an extension of the procedure introduced by Kohno, Bathe, and Wright for one-dimensional problems [1]. Specifically, the novelties are: two-dimensional problems are solved (and three-dimensional problems would be tackled similarly), a scheme is given to overcome ill-conditioning, the method is presented for time-dependent problems, and focus is on the solution of problems in solids and structures using real arithmetic only. The method combines advantages of finite element and spectral techniques, but an important point is that it preserves the fundamental properties of the finite element method. The general formulation of the procedure is given and various examples are solved to illustrate the capabilities of the proposed scheme.

© 2012 Elsevier Ltd. All rights reserved.

## 1. Introduction

The finite element method is known to be an effective numerical tool for the solution of boundary value problems on complex domains [2]. However, the standard finite element method is not very effective for the solution of wave propagation problems [2–4]. The errors introduced in wave propagation analyses using the piecewise polynomial approximations of standard techniques have been identified and analyzed, see e.g. [5–6]. In the case of time harmonic wave solutions, it is well-known that the accuracy of the numerical solution becomes rapidly worse with increasing wave number [2,7–10]. Therefore, for problems with short waves, very fine meshes are required to obtain reasonable solutions, so fine, that the numerical solution effort may be prohibitive. In the case of transient wave propagations, the solution may exhibit spurious oscillations, related to the Gibb's phenomenon, and the numerical wave propagation velocity may be significantly different from the physical velocity, due to the numerical period elongation and amplitude decay [2,11] resulting in the dispersion and dissipation errors [11–23]. When a wave travels long distances, the errors become large and the numerical solution is very inaccurate. Therefore, whenever high-frequency components are present in the loading, significant errors are present in the numerical solution unless the mesh is fine enough to model the rapid spatial variations. In addition, due to the mesh used, the computed wave velocities may also artificially depend on the propagation directions causing distortions in the waveforms. Hence, the discrete model behaves

anisotropically even though the mathematical model pertains to an isotropic medium. Indeed, just one badly distorted element may cause large solution errors.

A considerable amount of research has been focused on the development of the finite element method for wave propagation problems. For time harmonic wave problems, the partition of unity finite element method has been proposed for the solution of Helmholtz problems at high frequencies [24–27]. An important point is that in this method specific wave propagation solutions are incorporated into the solution space. However, when solving practical wave propagation problems, we frequently do not know a priori what waves and travels need to be predicted. In fact, the solution is a sum of unknown waves and propagations, and may also include wave conversions. Therefore, embedding *general* multiple wave patterns, like we propose below, into the solution space seems to be a more natural way of capturing the unknown wave solutions.

The *spectral method*, see Ref. [28], the *spectral element method*, see Refs. [29–36] and the *spectral finite element method*, see Refs. [37–40] and each time the references therein, have also been developed to solve wave propagation problems. Considering the literature, it is sometimes difficult to see whether a method belongs to one or another of these categories. However, in all cases higher-order polynomials or harmonic functions are used in the solution space.

The *spectral method* can be used to obtain numerical solutions very close to exact solutions because harmonic functions are used as basis functions and the solutions of wave equations are basically harmonic functions. However, the spectral method is difficult to use for geometrically complicated domains, as encountered in

\* Corresponding author.

E-mail address: [kjb@mit.edu](mailto:kjb@mit.edu) (K.J. Bathe).

practice, since the method uses global basis functions. Hence in the analysis of solids and structures, the method has found limited practical use. A natural extension is therefore the *spectral element method*. Here, in essence, high-order Lagrangian-based finite elements are used with special nodal positions and integration schemes that lead to diagonal mass matrices. The method shows low numerical dispersion with respect to standard finite element methods and can be very effective in explicit time integration but does not lend itself to modeling complex structures and to the hierarchical increase in the displacement interpolations that we pursue in this paper.

In addition, the *spectral finite element method* has been developed and is used effectively to solve certain wave propagation problems in that it approximates the solutions with trigonometric polynomials [37–40]. However, this method uses a transformation of the governing wave equations to the frequency domain, the solution in the frequency domain, and the back transformation to the time domain. The method is overall an expensive procedure and also difficult to extend to general nonlinear analysis.

A considerable attention has been given to the development of discontinuous finite element formulations [41–43]. These methods provide much generality for the solution of problems and can in particular be used for wave solutions. However, the methods are, in practice, not sufficiently effective because of the discontinuities between the elements that need to be dealt with, for example, using penalty factors. An extension of these techniques is the discontinuous enrichment method in which free-space solutions of the governing problem are used for each element in addition to the polynomial approximations [44,45]. Hence these methods too do not lend themselves to solve in a uniform and effective manner general linear and nonlinear problems in solid and structural mechanics.

Our approach presented in this paper is related to these methods but has some attributes that the above-mentioned methods do not offer. In Ref. [1], Kohno, Bathe, and Wright presented a valuable finite element scheme that combines advantages of the finite element and spectral methods. The essence of this scheme is that low-order finite elements enriched with harmonic functions are used. The amount of enrichment is chosen by the analyst, and results in additional element degrees of freedom. Hence, with no enrichment the traditional finite element method is used, but the method is attractive for wave propagation problems because additional harmonic functions are embedded when so desired. The application of boundary conditions is performed as in the standard finite element method and, indeed, all computations are as in the usual finite element procedure [2]. In Ref. [1], the method was applied to solve one-dimensional time-harmonic multiscale wave problems with waves of dramatically different lengths in different regions and with wave conversions. It was shown that, for the solution of one-dimensional problems, using the method gives considerably more accurate results than using the conventional finite element method for the same computational cost.

Of course, the general approach to enrich the traditional Lagrangian finite element basis functions with functions that can more accurately represent desired solutions, has been pursued for some decades [2]. This approach can be effective for the solution of specific problems. For example, for pipe analyses special functions were embedded that are known to represent more accurately pipe ovalization effects [46,47]. These elements result in much more accurate solutions in linear and nonlinear analyses. The same approach has been used, for example, in the development of beam elements to include warping effects [48], in fluid flow analyses to better capture the flow conditions [49,50], and in solid mechanics to predict locally nonsmooth features like needed for cracks, voids and failure [51,52]. In each of these cases, in essence, the ‘character’ of the solution sought is embedded in the solution space. Clearly, whenever specific problems are tackled,

an appropriate enrichment of the traditional finite element functions is of interest (as exposed in general in Ref. [24]). The method that we focus upon in this paper uses that approach and in that sense is, of course, related to formulations given earlier for wave propagations and other analyses.

The objective of this paper is to extend the specific procedure of Ref. [1] to solve multi-dimensional wave propagation problems. We provide a generally applicable enriched finite element scheme. The solution field is discretized with the usual Lagrangian functions plus harmonic functions within the elements that provide for additional element behavior and degrees of freedom.

In the following, in Section 2, we present the governing equations of the elastic wave propagation problems that we consider in this paper and the new finite element interpolation functions. A practical point is that these functions are formulated to avoid computations in complex arithmetic. We also discuss how to impose the boundary conditions, the use of the interpolations with distorted elements, and the problem of ill-conditioning of the governing algebraic equations. To overcome ill-conditioning, we introduce a simple computational scheme.

Then, in Section 3, we present the results of a range of numerical tests that illustrate the capabilities of the method. We consider the cases of time harmonic and transient scalar wave equations; the impact of an elastic bar against a rigid wall; a two-dimensional elastic transient wave propagation problem and the solution of a Helmholtz equation around a cylinder, both in infinite domains. For the transient analyses we use an implicit time integration and focus on the capabilities of the spatial discretization. It is seen that the finite element formulation can be used to control the numerical dispersion and dissipation by increasing the element degrees of freedom, and that accurate results can be obtained.

While we consider only two-dimensional linear problems in this paper, an important point is that the method can, in principle, also directly be extended to three-dimensional, beam, plate, shell and general nonlinear and multi-physics solutions – since the method is in fact just the standard finite element method enriched with specific functions and all fundamental properties of the standard method are applicable. However, significant further research is required to develop important features of the procedure in order to obtain computationally effective solutions, as we mention in the concluding remarks.

## 2. Formulation of the method

In this section we first present the governing equations of the physical problems considered, then the finite element procedure, and thereafter some important attributes of the solution technique.

### 2.1. Governing continuum mechanics equations

We consider an elastic, isotropic, homogeneous medium,  $V$ , occupying a domain in  $\mathbb{R}^3$ . The boundary of  $V$  is denoted by  $S$ . In order to model an unbounded domain, a “model boundary condition” is used on  $S_{ext}$ . The displacement is denoted by  $\underline{u}(\underline{x}, t)$  where  $\underline{x} \in V$ .

For isotropic elastic wave propagations, the equations of motion are

$$\rho \ddot{\underline{u}} = \nabla \cdot \underline{\tau}(\underline{u}) + \underline{f}^B \quad (1)$$

where  $\rho$  is the mass density,  $\underline{f}^B$  is the body force vector, and  $\underline{\tau}(\underline{u})$  is the stress tensor [2].

The equations of motion are completed with appropriate boundary conditions. As is usual, we split the boundary  $S$  into two parts  $S_u$  and  $S_f$  with the boundary conditions

$$\underline{u} = \underline{u}^{S_u} \quad \text{on } S_u \text{ (Dirichlet boundary)} \quad (2)$$

$$\underline{\tau}(\underline{u}) \cdot \underline{n} = \underline{f}^{S_f} \quad \text{on } S_f \text{ (Neumann boundary)} \quad (3)$$

Here  $\underline{u}^{S_u}$  is the prescribed displacement,  $\underline{n}$  is an outward unit normal vector on  $S_f$ , and  $\underline{f}^{S_f}$  is the imposed boundary traction vector.

Included in  $S_f$  is the boundary,  $S_{ext}$ , used to model an unbounded domain, on which we use

$$\underline{f}^{S_f} = -c_L \rho [\underline{v} \cdot \underline{n}] \underline{n} - c_T \rho \underline{v}_T \quad (4)$$

Here  $\underline{v}_T = \underline{v} - [\underline{v} \cdot \underline{n}] \underline{n}$  is the velocity tangent to the surface and  $c_L$  and  $c_T$  are the  $P$  and  $S$  wave velocities, respectively.

## 2.2. Variational form of the governing continuum mechanics equations

Multiplying Eq. (1) by a virtual displacement  $\underline{\bar{u}}$  and integrating by parts over  $V$  we obtain in the standard way the principle of virtual displacements [2]

$$\int_V \bar{\underline{\epsilon}}^T \underline{\tau} dV + \int_V \rho \underline{\bar{u}}^T \underline{\ddot{u}} dV = \int_{S_f} \underline{\bar{u}}^T \underline{f}^{S_f} dS + \int_V \underline{\bar{u}}^T \underline{f}^B dV \quad (5)$$

where  $\underline{\bar{u}}$  is the virtual displacement and  $\bar{\underline{\epsilon}}$  is the corresponding virtual strain. The important point is that for the method we propose, the usual standard procedures of finite element analysis are used. Hence, regarding the finite element formulation the only – but important – novelty is the use of the specific interpolation functions given next.

## 2.3. Element interpolation functions

While we next consider the two-dimensional analysis of solids, the basic equations can directly be generalized to plate, shell and three-dimensional solutions. The element interpolation functions for Eq. (5) are for two-dimensional analyses given by – considering only one typical solution variable  $u$

$$u(r, s) = \sum_{\alpha} h_{\alpha}(r, s) \left[ U_{(\alpha, 0, 0)} + \sum_{k_x=1}^n \left\{ \cos\left(\frac{2\pi k_x x}{\Lambda_x}\right) U_{(\alpha, k_x, 0)}^C + \sin\left(\frac{2\pi k_x x}{\Lambda_x}\right) U_{(\alpha, k_x, 0)}^S \right\} + \sum_{k_y=1}^m \left\{ \cos\left(\frac{2\pi k_y y}{\Lambda_y}\right) U_{(\alpha, 0, k_y)}^C + \sin\left(\frac{2\pi k_y y}{\Lambda_y}\right) U_{(\alpha, 0, k_y)}^S \right\} \right. \\ \left. + \sum_{k_x=1}^n \sum_{k_y=1}^m \left\{ \cos\left(\frac{2\pi k_x x}{\Lambda_x} + \frac{2\pi k_y y}{\Lambda_y}\right) U_{(\alpha, k_x, k_y)}^{C+} + \sin\left(\frac{2\pi k_x x}{\Lambda_x} + \frac{2\pi k_y y}{\Lambda_y}\right) U_{(\alpha, k_x, k_y)}^{S+} \right. \right. \\ \left. \left. + \cos\left(\frac{2\pi k_x x}{\Lambda_x} - \frac{2\pi k_y y}{\Lambda_y}\right) U_{(\alpha, k_x, k_y)}^{C-} + \sin\left(\frac{2\pi k_x x}{\Lambda_x} - \frac{2\pi k_y y}{\Lambda_y}\right) U_{(\alpha, k_x, k_y)}^{S-} \right\} \right] \quad (6)$$

where the  $U_{(\alpha, k_x, k_y)}$  with superscripts are the nodal degrees of freedom; here the  $S$ ,  $C$  and  $+$  and  $-$  are used in the superscripts to correspond to the harmonic expressions. In one-dimensional solutions, Eq. (6) is simply [1]

$$u(r) = \sum_{\alpha} h_{\alpha}(r) \left[ U_{(\alpha, 0)} + \sum_{k_x=1}^n \left\{ \cos\left(\frac{2\pi k_x x}{\Lambda_x}\right) U_{(\alpha, k_x)}^C + \sin\left(\frac{2\pi k_x x}{\Lambda_x}\right) U_{(\alpha, k_x)}^S \right\} \right] \quad (7)$$

In Eq. (6),  $x$  and  $y$  are the coordinates at any point of the element and  $h_{\alpha}$  is the conventional finite element interpolation function with  $\alpha$  the local node number of the element. Hence for a 4-node element we have  $\alpha = 1, \dots, 4$ , and for a 9-node element we have  $\alpha = 1, \dots, 9$ . These conventional interpolation functions are enriched by harmonic functions to obtain the actual interpolations used for the displacements. Of course, these interpolation functions can be written using exponentials on the complex plane, but since we consider the solution of solids we mostly use real arithmetic (see Section 3.5 for an exception) which can be much more effective.

For the geometry interpolation of the elements, we use the original functions  $h_{\alpha}$  in the natural  $(r, s)$  space.

In Eq. (6), the  $\Lambda_x$  and  $\Lambda_y$  are fundamental wavelengths, and  $k_x$  and  $k_y$  are integers in the range of  $1 \leq k_x \leq n$ ,  $1 \leq k_y \leq m$ , respectively, where  $n$  and  $m$  are the cutoff numbers for each term. The analyst needs to choose these data, as part of the finite element model definition, for the problem solution. In our current work, and in all solutions given in Section 3, we have so far used  $\Lambda_x = 2\Delta x$  and  $\Lambda_y = 2\Delta y$ , where  $\Delta x$  and  $\Delta y$  are typical element sizes. This choice is physically appropriate and has also some mathematical basis, see Ref. [1].

Considering the integers  $n$  and  $m$ , values between 1 and 3 are most appropriate as exemplified in Section 3. Here we should note that it is not necessary to use  $n = m$  but if done, the functions not needed will simply not add additional solution accuracy as it is always the case in finite element analysis.

Of course, the elements used with the interpolation functions in Eq. (6) satisfy the rigid-body mode criteria and the patch tests [2].

## 2.4. Imposing boundary conditions

The way we impose boundary conditions is explained in detail in Ref. [1]. Here it is important to note that in this finite element scheme the nodal values  $U_{(\alpha, k_x, k_y)}$  contain the effect of the harmonic functions. Hence to exactly satisfy the displacement boundary conditions, we choose the following values

$$U_{(\alpha, k_x, k_y)} = u^{S_u} \quad \text{for } k_x = 0 \quad \text{and } k_y = 0 \quad (8)$$

$$U_{(\alpha, k_x, k_y)} = 0 \quad \text{for } k_x \neq 0 \quad \text{or } k_y \neq 0 \quad (9)$$

where  $u^{S_u}$  is the prescribed displacement. Therefore we impose the boundary displacements not using the harmonic functions. For the Neumann boundary conditions, the boundary term in the discretized equations is calculated in the same way as in the standard finite element method.

## 2.5. Geometrically distorted elements

To evaluate the coefficient matrices, analytical integration (as used in Ref. [1]) can directly be used as long as the elements are rectangular. If the elements are slightly distorted, a semi-analytical integration may still be possible. However, when the element distortions are significant, numerical integration is probably necessary. In this research we simply used the conventional Gauss-Legendre integration scheme [2]. While we use this scheme it is clear that more efficient techniques are very desirable (see Section 4).

To test the performance of the elements when these are distorted, we solve a simple problem in the domain  $[0, 1] \times [0, 1]$  for which the exact solution is  $u(x, y) = \sin(4\pi x)$ , see Fig. 1(a). Fig. 1(b) shows a distorted  $10 \times 10$  mesh using 4-node elements. Here, the distortion ratio is defined as the ratio of the longest side length of any of the elements over the shortest side length of any of the elements in the domain [2].

In the study we use the  $10 \times 10$  mesh of 4-node elements and a  $5 \times 5$  mesh of 9-node elements (simply geometrically combining four 4-node elements to one 9-node element) which leads to the

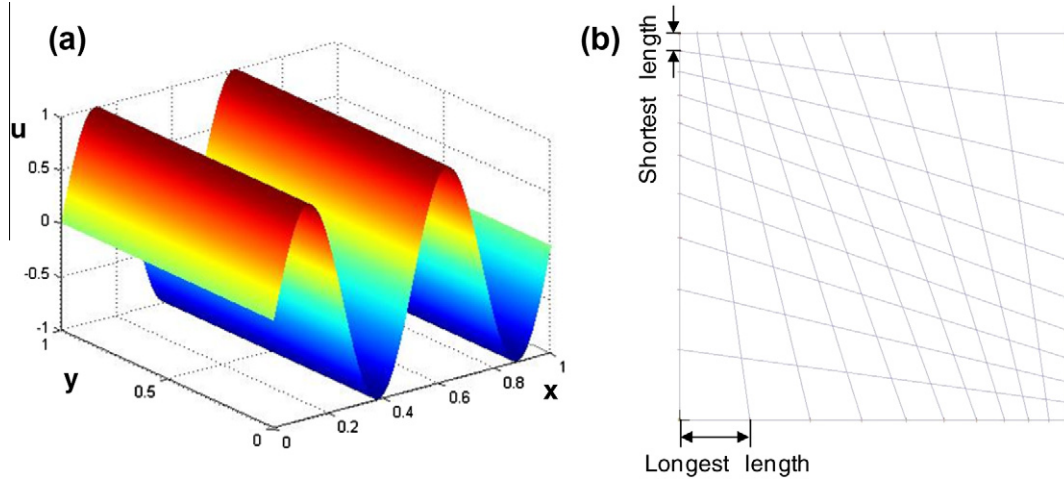


Fig. 1. (a) Analytical solution of problem considered; (b)  $10 \times 10$  mesh of 4-node elements with distortion ratio = 4.

same number of total degrees of freedom, and  $(n, m) = (2, 2)$  for the cutoff numbers. Fig. 2 shows the results obtained using the 4-node and 9-node element meshes. Note that the numerical result using the 9-node enriched element is very similar to the analytical solution even for the largest distortion ratio.

Fig. 3 shows the relative error in the  $L^2$  norm, in percent, defined as

$$\frac{\left( \int_V |u - u_h|^2 dV \right)^{\frac{1}{2}}}{\left( \int_V |u|^2 dV \right)^{\frac{1}{2}}} \times 100 \quad (10)$$

While the 4-node enriched element is quite sensitive to distortion, the 9-node enriched element is not that sensitive and hence performs much better.

This result can be explained by the loss of predictive capability of the elements due to element geometric distortions, which is discussed in Refs. [2,53].

## 2.6. A scheme to overcome the (possible) ill-conditioning of the algebraic equations

In earlier research on the partition of unity finite element and generalized finite element methods, it was reported that the resulting interpolation functions can lead to singular matrices or to ill-conditioning of the system of linear equations. The singularity occurs because some interpolation functions are linearly dependent, and the ill-conditioning occurs because the interpolation functions used are “close” to each other. With Eq. (6), the functions

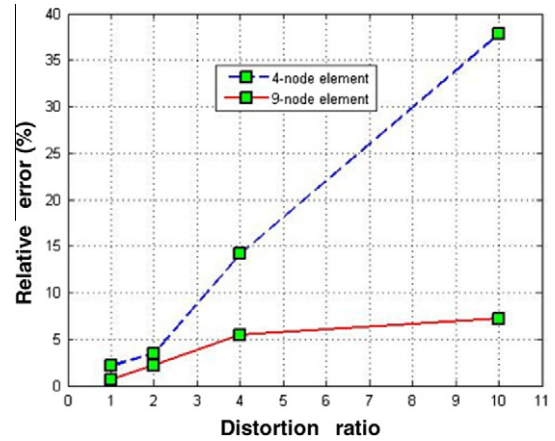


Fig. 3. Relative error in  $L^2$  norm using enriched elements.

are linearly independent but do become close to each other as the cutoff numbers become large.

Strouboulis et. al. [51] proposed to change the stiffness matrix slightly, and then iterate in order to annihilate the resulting error. However, our aim is to not iterate and, also, to have a scheme that lends itself to nonlinear analysis, in which exact tangent stiffness matrices change and may become singular (for physical reasons). Hence we change the mass matrix, rather than the stiffness matrix,

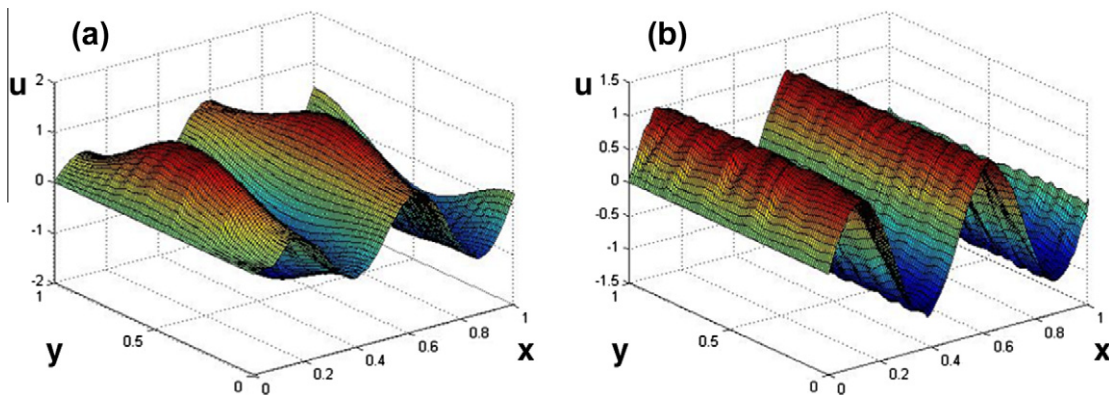


Fig. 2. Numerical solutions using (a) the 4-node enriched element and (b) the 9-node enriched element; the distortion ratio = 10.



and use in the time integration on the left-hand side of the algebraic equations

$$\underline{M} = (1 - \alpha)\underline{M}_{consistent} + \alpha\underline{M}_{lumped} \quad (11)$$

and on the right-hand side of the equations

$$\underline{M} = \underline{M}_{consistent} \quad (12)$$

where  $\alpha$  is a parameter of very small magnitude, and we calculate the lumped mass matrix  $\underline{M}_{lumped}$  using the total mass and allocating the lumped masses in the ratio of the diagonal elements of the consistent mass matrix. Specific results using this scheme are given in Section 3.2. Note that the mass matrix in Eq. (11) is only used to overcome a possible ill-conditioning of the coefficient matrix and not to reduce artificial dispersion or dissipation.

### 3. Numerical examples

In this section, we illustrate the performance of the enriched finite element method by solving several wave propagation problems. First, we solve time harmonic and transient scalar wave equations and focus on the numerical dispersion. Then, we use the method to solve for the stress wave in the impact of an elastic bar and focus on the sharpness of the wave front. Third, an elastic wave propagation problem is solved which contains  $P$ ,  $S$  and Rayleigh waves. Finally, we use the method to predict the propagation

of an acoustic pressure wave, originating from a circular cylinder, in an infinite domain.

For all transient analyses we use implicit time integration – which is not mostly employed in practical wave analyses. However, using implicit time integration provides a stringent test on the spatial discretization scheme and when employed in practice can be more reliable [2].

#### 3.1. Solution of time harmonic scalar wave

For the problem considered, the solution for  $u$  is governed by

$$\frac{\partial^2 u}{\partial x^2} + \frac{\partial^2 u}{\partial y^2} + k^2 u = 0, \quad 0 \leq x \leq 2 \quad \text{and} \quad 0 \leq y \leq 2 \quad (13)$$

with the boundary conditions

$$\begin{aligned} u(0, y) = 0, \quad \frac{\partial u(x, 2)}{\partial y} = 0, \quad \frac{\partial u(x, 0)}{\partial y} = 0, \\ \frac{\partial u(2, y)}{\partial x} = 4\pi \quad (\text{and} = 8\pi \text{ for case 2}) \end{aligned} \quad (14)$$

where  $k = 8\pi$  ( $32\pi$ ) in  $0 \leq x \leq 1$  and  $k = 4\pi$  ( $8\pi$ ) in  $1 \leq x \leq 2$  for the case 1 (case 2). In Fig. 4, we present the exact solutions of  $u$  for both cases. This is, of course, really only a one-dimensional problem but it is a useful problem to study the errors occurring in numerical schemes.

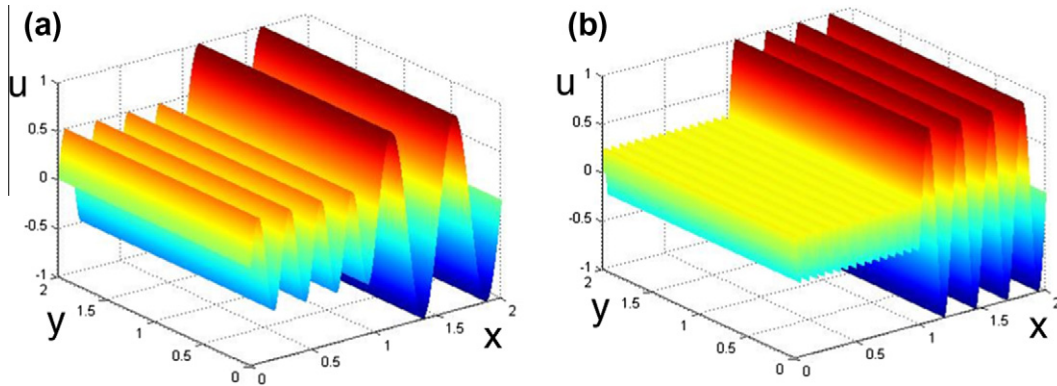


Fig. 4. Analytical solutions for problems considered (a) case 1; (b) case 2.

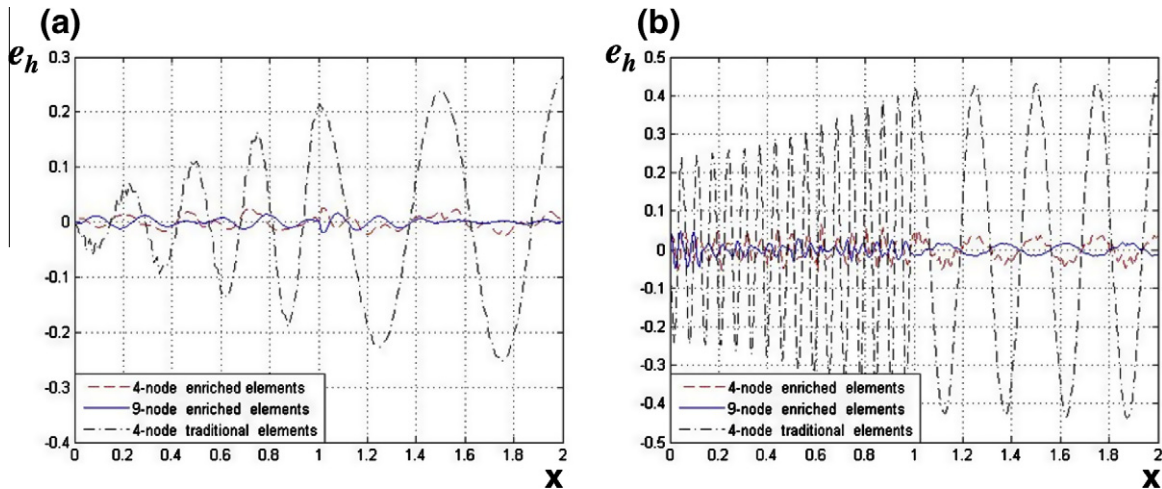


Fig. 5. Solution errors using uniform meshes: (a) case 1, using 80 linear elements of the conventional finite element method; 8 linear enriched elements with cutoff number 2; 4 quadratic enriched elements with cutoff number 3; (b) case 2, using 320 linear elements of the conventional finite element method; 20 linear enriched elements with cutoff number 3; 16 quadratic enriched elements with cutoff number 3.

In Fig. 5, we study the error  $e_h = u(x,0) - u_h(x,0)$  using equal-sized elements in each solution. The error in the finite element solution is due to the numerical period elongation and amplitude decay, also referred to as numerical dispersion and dissipation. Analyses of these errors are given, for example, in Refs. [2,7–11].

We see that in these cases the 4-node and 9-node enriched elements perform very well.

### 3.2. Solution of transient scalar wave

The scalar wave equation with a Ricker wavelet source at the center of a two-dimensional domain, as considered in Ref. [21], is given by

$$\frac{\partial^2 u}{\partial x^2} + \frac{\partial^2 u}{\partial y^2} + F(0,0,t) = \frac{1}{c^2} \frac{\partial^2 u}{\partial t^2} \quad (15)$$

$$F(0,0,t) = 10 \left( 1 - 2\pi^2 f^2 (t - 0.25)^2 \right) \exp \left( -\pi^2 f^2 (t - 0.25)^2 \right) \quad (16)$$

where  $u$  is the displacement solution sought,  $c$  is the wave velocity,  $f$  is the central frequency and in this example  $c = 1$  and  $f = 6$  Hz. Only the domain  $[0,1] \times [0,1]$  shown in Fig. 6 is used for the finite element solution because of symmetry. While, in general, absorbing boundary conditions should be prescribed at the outer boundary, in this solution no “absorbing” boundary conditions are used because for the time considered 0.95 s, the wave does not reach this boundary. With the conventional finite element method, an  $80 \times 80$  4-node element mesh is employed, leading to 6,561 degrees of freedom. For the enriched method, an  $8 \times 8$  4-node element mesh with cutoff numbers  $(n,m) = (1,1), (2,2), (3,3)$  is used, leading to 729, 2,025, and 3,969 degrees of freedom, respectively. In all solutions, we used the trapezoidal rule of time integration, with a very small time step  $\Delta t = 0.00625$  s, which corresponds to a CFL number = 0.5 for the  $80 \times 80$  mesh. To assess the accuracy of the solution, we also solved the problem with the  $8 \times 8$  mesh of 4-node elements and  $(n,m) = (4,4)$  and obtained negligible differences to the response calculated with  $(n,m) = (3,3)$ , see Fig. 7.

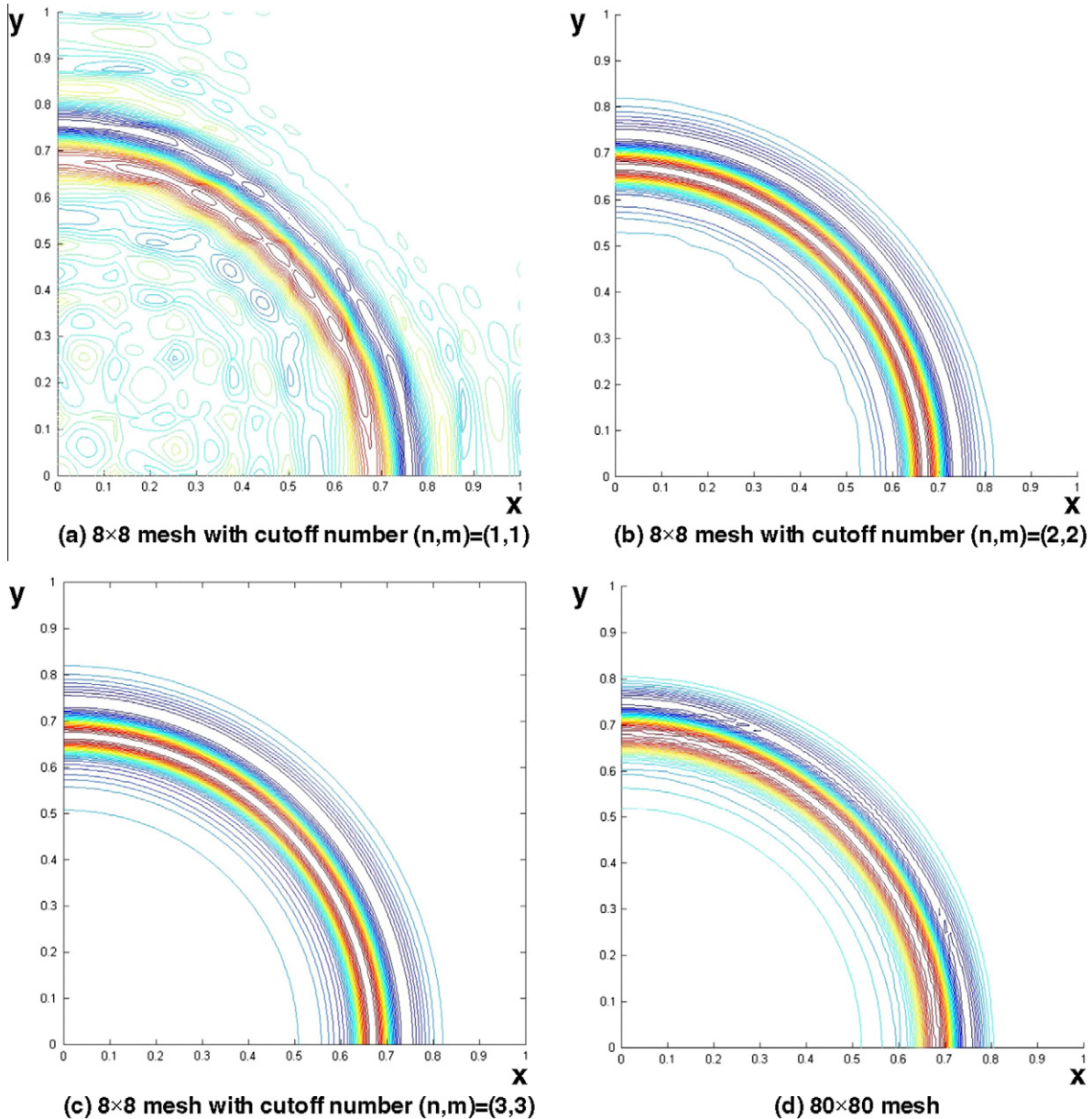


Fig. 6. Snapshots of displacements at  $t = 0.95$  s with various cutoff numbers.

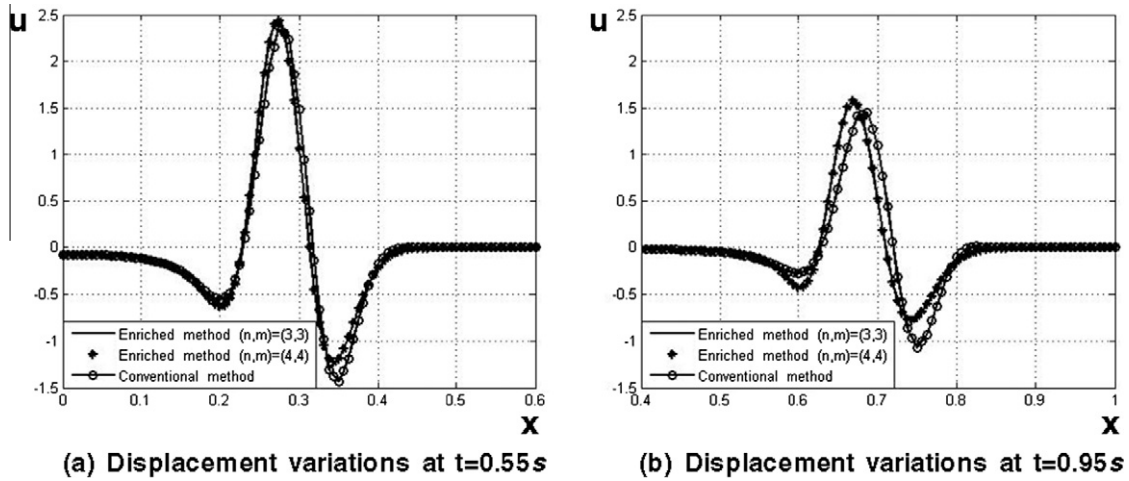


Fig. 7. Displacement variations along the  $x$ -axis at two times.

Fig. 6 gives snapshots of the displacements at time  $t = 0.95$  s as calculated using the conventional and enriched methods. As expected, the numerical results of the enriched method exhibit better accuracy as the cutoff number increases. Also, for the meshes used, the conventional method gives results that are not as good as obtained with the enriched method with the cutoff number  $(n, m) = (3, 3)$ . Considering the displacement variations along the  $x$ -axis [21], as shown in Fig. 7, the error in the response prediction increases, using the traditional method, with the distance of wave travel in the computational domain. As well known, even an apparently small error in wave propagation velocity may result into

Table 1

Condition number of coefficient matrix (largest eigenvalue/ smallest eigenvalue [2]) for various cutoff numbers and values of  $\alpha$  using the  $8 \times 8$  mesh of 4-node enriched elements.

Cutoff number	8 $\times$ 8 Mesh of 4-node enriched elements			
	Condition number			
	$(\alpha = 0)$	$(\alpha = 0.000001)$	$(\alpha = 0.00001)$	$(\alpha = 0.0001)$
$(n, m) = (1, 1)$	5.8E+07	3.6E+07	1.1E+07	1.7E+06
$(n, m) = (2, 2)$	3.4E+10	1.2E+09	1.5E+08	1.7E+07
$(n, m) = (3, 3)$	9.7E+12	4.0E+09	4.0E+08	4.2E+07
$(n, m) = (4, 4)$	2.8E+16	8.1E+09	8.3E+08	7.8E+07

unacceptable displacement and hence stress errors as time increases.

We obtained the results given above without regard to ill-conditioning of the coefficient matrix. However, as pointed out in Section 2.6, using the displacement interpolation functions of Eq. (6) can lead to ill-conditioning and indeed in this problem solution, ill-conditioning can be seen when calculating the condition number (although the solution is obtained in this case without numerical difficulties even when  $(n, m) = (4, 4)$ ). Table 1 lists the condition number of the coefficient matrix using various cutoff numbers and values of  $\alpha$  in Eq. (11). Fig. 8 shows the relative solution errors calculated over the domain in the  $L^2$  norm when using different parameters, and also the displacements along the  $x$ -axis obtained with  $(n, m) = (4, 4)$ . As seen, when using  $\alpha = 0.00001$  the condition number is much improved while the error due to using this value of  $\alpha$  can be neglected.

### 3.3. One-dimensional impact of an elastic bar

A good benchmark problem for testing a finite element method for wave propagation solutions is the one-dimensional impact problem shown in Fig. 9 [23].

The problem can, of course, be solved very accurately using explicit time integration, lumped mass matrices, and meshes of

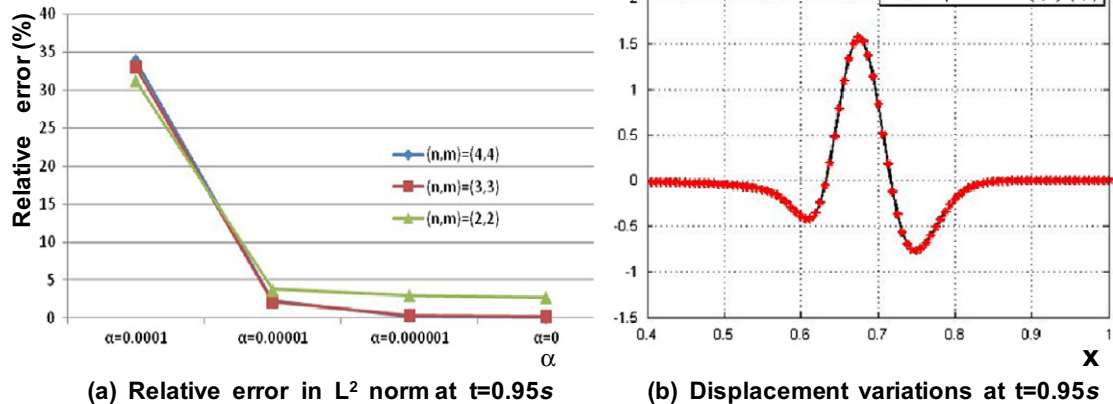
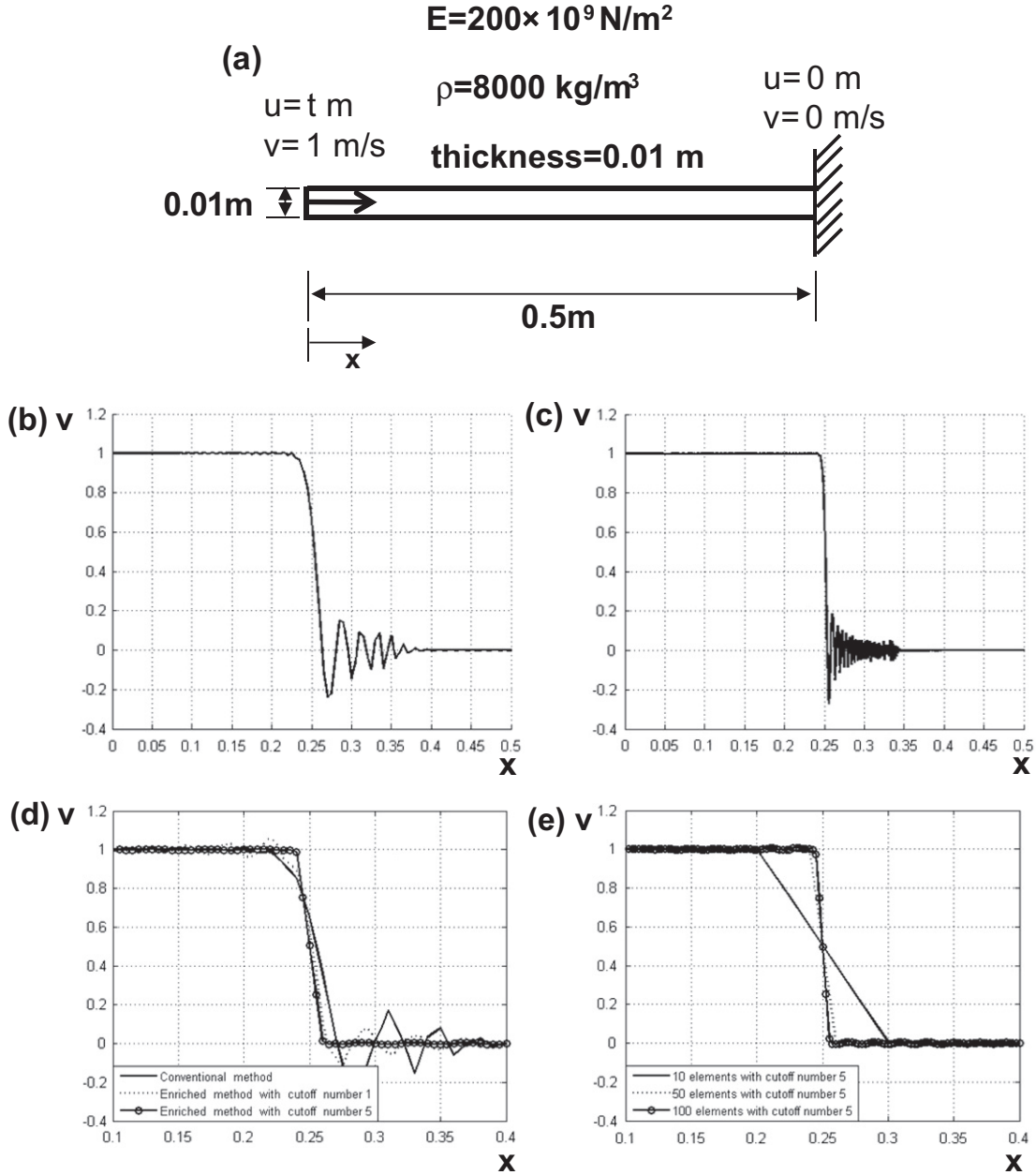


Fig. 8. Study of solution accuracy at time  $t = 0.95$  s; (a) Relative errors in  $L^2$  norm for various cutoff numbers and values of  $\alpha$ , the solution using  $\alpha = 0$  and  $(n, m) = (4, 4)$  is used as the solution to compare with; (b) comparison of the numerical solutions obtained using  $\alpha = 0$  and  $\alpha = 0.00001$ .





**Fig. 9.** Solution of impact of a bar at time 0.00005 s using uniform meshes; (a) elastic bar considered; (b) velocity distribution calculated using 100 traditional linear elements; (c) solution using 700 traditional linear elements (d) solutions using 50 linear enriched elements with cutoff numbers 0, 1, 5; (e) solutions using the cutoff number 5 with 10, 50, 100 linear enriched elements.

2-node linear elements [2]. To test the proposed formulation, we solve the problem using uniform meshes of linear elements, consistent mass matrices, and in each case, we use the trapezoidal rule of time integration with the very small time step  $\Delta t = 2.5 \times 10^{-8} \text{ s}$ .

Fig. 9 gives the results obtained. As well known, using the traditional finite element discretizations, spurious oscillations in the stress and velocity predictions are obtained. These oscillations are somewhat reduced using the time integration method proposed by Bathe [54] but are still present. As seen in the figure, when we use the enriched finite element method, we can control the spurious high-frequency oscillations and make them acceptably small. As mentioned already, we used the consistent mass matrix, although in certain analyses, using a lumped mass matrix or a combination of lumped and consistent mass matrices might reduce the errors [55].

### 3.4. Solution of two-dimensional P, S and Rayleigh waves

In this section, we solve the Lamb problem of elastic waves propagating inside a semi-infinite domain due to an imposed surface vertical force [56], as considered in refs. [30,31].

From Eq. (5), the finite element formulation gives for an element [2]

$$\int_{V^{(m)}} \underline{H}^{(m)T} \begin{bmatrix} \rho & 0 \\ 0 & \rho \end{bmatrix} \underline{H}^{(m)} dV^{(m)} \ddot{\underline{U}} + \int_{S_{ext}^{(m)}} \underline{H}^{(m)T} \begin{bmatrix} \rho c_L & 0 \\ 0 & \rho c_T \end{bmatrix} \underline{H}^{(m)} dS^{(m)} \dot{\underline{U}} + \int_{V^{(m)}} \underline{B}^{(m)T} \underline{C}^{(m)} \underline{B}^{(m)} dV^{(m)} \underline{U} = \int_{S_f^{(m)}} \underline{H}^{(m)T} \underline{f}_{S_f^{(m)}} dS^{(m)} \quad (17)$$

where  $\underline{H}^{(m)}$  is the displacement interpolation matrix obtained from Eq. (6),  $\underline{B}^{(m)}$  is the corresponding strain-displacement matrix, and



$\underline{C}^{(m)}$  is the constitutive matrix for the plane strain condition used. Note that the boundary condition to model the infinite domain, Eq. (4) for  $S_{ext}$ , results into the velocity dependent term in Eq. (17).

The isotropic semi-infinite elastic medium has a  $P$ -wave velocity 3200 m/s, an  $S$ -wave velocity 1847.5 m/s a mass density 2200 kg/m<sup>3</sup>, and is modeled as a domain of size 4000 × 2000 m<sup>2</sup> in plane strain conditions, see Fig. 10. The force, a Ricker wavelet with a central frequency of 14.5 Hz, is applied on the free surface at  $(x_A, y_A) = (2000 \text{ m}, 2000 \text{ m})$ . Two receivers are located at 640 m and 1280 m from the applied force. For the numerical solution, we use a mesh of 50 × 25 4-node enriched elements, with

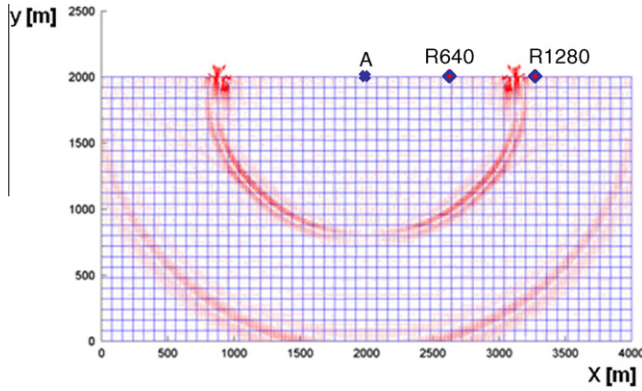


Fig. 10. Wave profiles at time 0.72 s showing the Rayleigh, P and S waves in Lamb's problem. Point A indicates the applied force position, and R640 and R1280 indicate the positions of the receivers.

$(n, m) = (2, 2)$  leading to a total of 66,300 degrees of freedom, a consistent mass matrix, and the trapezoidal rule of time integration with a time step 0.0008 s. The total time of response to be calculated is 1 s; hence the  $P$  wave will reach the outer boundary during the solution time.

Fig. 10 shows the wave profiles at time 0.72 s, a strong Rayleigh wave along the surface and the  $P$  and  $S$  waves inside the domain. Fig. 11 gives the numerical prediction at the two receivers, which is in good agreement with the analytical solution. Note that in the finite element solution presented here, we did not incorporate any knowledge of the two waves a priori – this response was naturally solved for by use of our displacement interpolation functions, see Eq. (6). These displacement functions can naturally represent many different waveforms and will automatically solve for the actual wave response.

### 3.5. Solution of time harmonic acoustic pressure wave

Consider an inviscid fluid for which we define the velocity potential  $\phi$  with

$$\underline{v} = \nabla \phi, \quad p = -\rho \dot{\phi} \quad (18)$$

where  $\underline{v}$  is the velocity and  $p$  is the pressure [2]. The equation governing the pressure behavior is

$$\nabla^2 p = \frac{1}{c^2} \frac{\partial^2 p}{\partial t^2} \quad (19)$$

with the wave speed  $c = \sqrt{\beta/\rho}$  where  $\beta$  is the bulk modulus and  $\rho$  is the density of the fluid. Focusing on the propagation of a

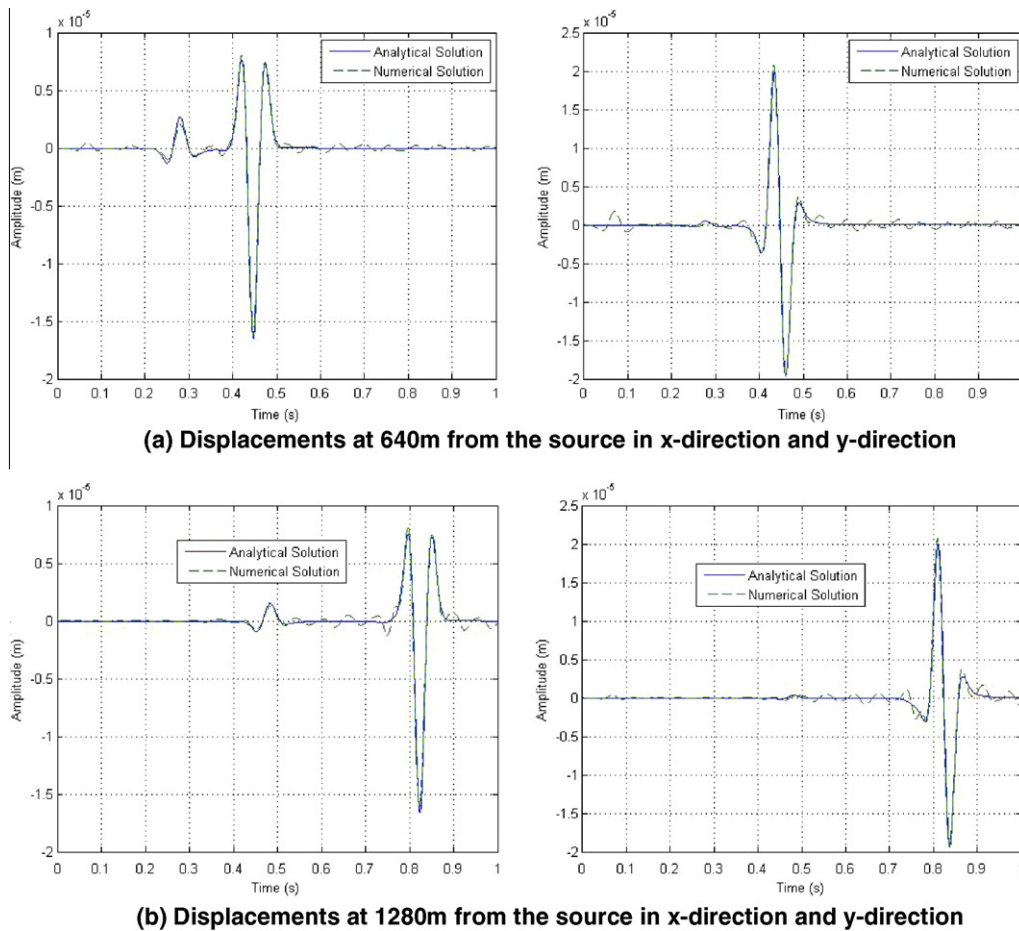


Fig. 11. Time history of displacement variations in x-direction and y-direction at the two receivers, numerical versus analytical results.

two-dimensional acoustic pressure wave at a single frequency, the time dependent pressure  $p$  can be written as [57–59]

$$p(x, y, t) = \text{Re}[P(x, y)e^{-i\omega t}] \quad (20)$$

Substituting from Eq. (20) into Eq. (19) we obtain the Helmholtz equation for the time harmonic pressure  $P$ . For the numerical test, we consider a circular cylinder with boundary  $S_f$  placed in the un-

bounded domain  $V$  (see Fig. 12). Our goal is to solve the Helmholtz problem like in Ref. [60]:

$$\begin{aligned} \nabla^2 P + k^2 P &= 0 \quad \text{in } V, \\ \frac{\partial P}{\partial n} &= g(x, y) \quad \text{on } S_f, \\ \lim_{r \rightarrow \infty} \sqrt{r} \left( \frac{\partial P}{\partial r} - ikP \right) &= 0 \end{aligned} \quad (21)$$

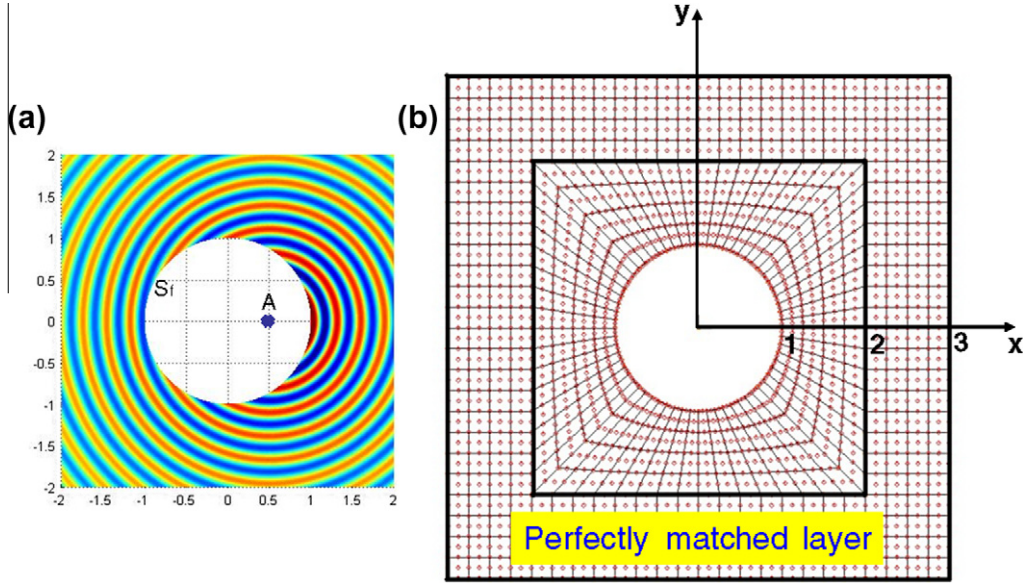


Fig. 12. Solution of pressure wave (a) the analytical pressure,  $A$  is at  $(x_0, y_0) = (0.5, 0)$ ; (b) mesh of 9-node elements used including the perfectly matched layer.

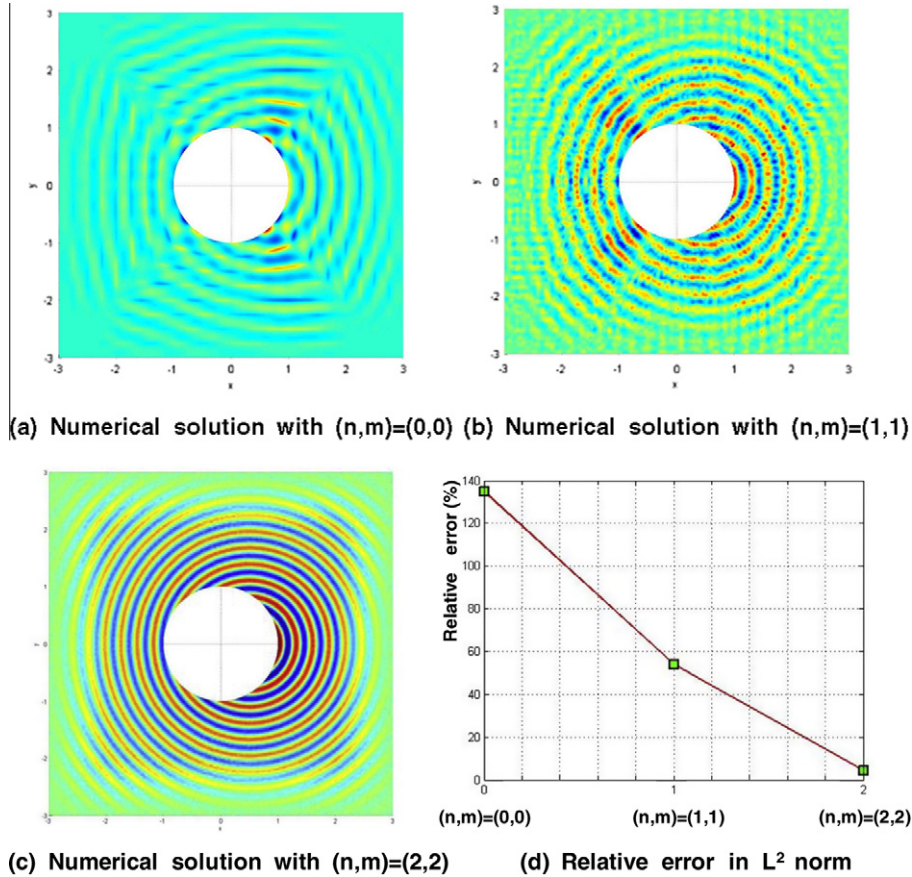


Fig. 13. Numerical solutions including the perfectly matched layer, and relative error in  $L^2$  norm not including the perfectly matched layer as a function of the cutoff number.

where  $k = \omega/c$  and  $r$  is the distance from the origin in the Cartesian coordinates (Fig. 12).

Considering this problem, the Hankel function of the first kind satisfies the first and third equations

$$P(x, y) = \frac{i}{4} H_0^{(1)} \left( k \sqrt{(x - x_0)^2 + (y - y_0)^2} \right) \quad (22)$$

Hence using this function to prescribe  $g = \partial P / \partial n$  on the boundary  $S_f$ , Eq. (22) is the exact solution for the Helmholtz problem in Eq. (21). Using  $x_0 = 0.5$ ,  $y_0 = 0$ , the radius of the circular cylinder = 1, like in Ref. [60], and  $k = 22.06$ , Fig. 12(a) shows the analytical solution of the pressure.

In the finite element solution we prescribe the boundary condition  $g = \partial P / \partial n$  on the cylindrical boundary  $S_f$  and calculate the pressure response in the computational domain.

To model the infinity of the physical domain, we use the perfectly matched layer of Ref. [60] with the recommended parameters. This layer truncates the unbounded domain in the numerical calculation by the following equations

$$\frac{1}{\gamma_1} \frac{\partial}{\partial x} \left( \frac{1}{\gamma_1} \frac{\partial P}{\partial x} \right) + \frac{1}{\gamma_2} \frac{\partial}{\partial y} \left( \frac{1}{\gamma_2} \frac{\partial P}{\partial y} \right) + k^2 P = 0 \quad (23)$$

where

$$\gamma_1 = \begin{cases} 1 & \text{for } |x| < 2 \\ 1 + \frac{i}{k(3-|x|)} & \text{for } 2 \leq |x| \leq 3 \end{cases} \quad \text{and} \quad \gamma_2 = \begin{cases} 1 & \text{for } |y| < 2 \\ 1 + \frac{i}{k(3-|y|)} & \text{for } 2 \leq |y| \leq 3 \end{cases} \quad (24)$$

Fig. 12(b) shows the complete finite element domain meshed with 9-node elements, giving a total of 576 degrees of freedom when  $(n, m) = (0, 0)$ .

Fig. 13 gives contour plots of the pressure numerical solutions using the cutoff numbers from 0 to 2, where the result obtained using the cutoff numbers  $(n, m) = (2, 2)$  is in good agreement with the analytical solution.

As expected, the relative error in the  $L^2$  norm decreases as the cutoff number increases, see Fig. 13, and only a few harmonic functions need to be included to obtain sufficiently accurate results. If the numerical solution for a higher wave number  $k$  is to be obtained, it would be necessary to either increase the number of elements or the cutoff number in order to have the same level of solution accuracy.

We note that while in all previous solutions, we only used real arithmetic, in this example solution, we employed complex arithmetic for the perfectly matched layer in the discretized domain.

#### 4. Concluding Remarks

A finite element method for solving wave propagation problems in solids has been presented. The method is used as the traditional finite element procedures, but simply additional degrees of freedom (corresponding to the harmonic terms) are added to the nodes of lower- or higher-order standard elements. In many cases, only real arithmetic is employed. We have illustrated the use of the method in two-dimensional solutions, but the concept directly applies to three-dimensional solutions as well.

The method does not embed 'a priori' specific wave solutions, instead the procedure is a general scheme that directly and automatically gives the 'best' solution possible in the assumed solution space – just like the standard displacement-based finite element method by its minimization properties [2]. Therefore, like in the

standard finite element method, the assumed solution space must be rich enough to obtain an accurate approximation to the exact solution, and this means that the mesh must be fine enough and the number of harmonics used must be large enough. In this way, based on our numerical experiences thus far, accurate solutions can be obtained with reasonable meshes and solution data.

The method can be used with no enrichment functions (thus being the traditional finite element method) and thereafter harmonics to enrich the solution space can be selectively added, in an hierarchical manner [61]. This makes the method flexible and attractive for practical usage.

There are a number of items that should be tackled in further research on the method. In this paper we focused on the capability of the method to spatially resolve the desired solution and did not focus on the effectiveness with respect to computational cost. Hence further research should primarily focus on reaching cost effectiveness when using the method.

For transient analyses, we have employed the method with a consistent mass matrix and implicit time integration schemes, and obtained accurate solutions. However, the use of lumped mass approximations and explicit time integration, typically used for wave propagation solutions, should be explored.

The numerical integration of the stiffness and mass matrices should be studied in detail with the aim to find optimal schemes. We used the standard Gauss integration rules with many integration stations on the elements as the cutoff number increases. The element matrices have a specific structure that perhaps can be exploited for effective partial-analytical and numerical evaluations.

The number of degrees of freedom of the elements increases rapidly as the cutoff number increases. For example, considering a two-dimensional wave solution such as in Section 3.4, the numbers of degrees of freedom per node are 18, 50, 98 when using  $n = m = 1$ ,  $n = m = 2$ , and  $n = m = 3$ , respectively. Hence, the order of an element stiffness matrix becomes rapidly large as the cutoff number is increased, and the bandwidth of an assembled stiffness matrix can be very large, in particular in three-dimensional analyses. In explicit time integration, a large bandwidth does not result in computational difficulties, but in implicit integration, an iterative solution of the equations may need to be pursued.

In practice, the method may be most effective when used with only  $n = m = 1, 2$  or 3. The problem of ill-conditioning is then not as severe. We proposed a simple scheme to remedy ill-conditioning, but further research may lead to more effective schemes.

Theoretical convergence analyses should be pursued that include the effect of element sizes, fundamental wavelengths, and the number of harmonics used. Such analyses would give guidelines as to how best solve a given problem and may also lead to error estimates on the solution obtained (using the hierarchical features of the method) [62].

While we have presented the method for the displacement-based method of finite elements – with all the important properties directly applicable [2] – it would be valuable to extend the method for the  $u/p$  formulation (for incompressible analysis) and the MITC formulations for beams, plates and shells [2,63–65]. Then the influence of the enrichment functions on the satisfaction of the inf-sup condition needs to be investigated [66]. The method probably has good potential for the analysis of general shell structures, and also for the solution of multi-physics problems including fluid-structure interactions and electromagnetic effects [67].

Finally, since the method does not use specific analytical solutions – but “works like” the standard finite element method – the method can be extended to the solution of nonlinear problems, in particular problems with material nonlinearities [2]. However, the solution of large deformation problems, like encountered in crash analyses [68], would provide a particular challenge.



## References

- [1] Kohno H, Bathe KJ, Wright JC. A finite element procedure for multiscale wave equations with application to plasma waves. *Comput Struct* 2010;88:87–94.
- [2] Bathe KJ. Finite element procedures. Prentice Hall; 1996.
- [3] Harari I. A survey of finite element methods for time-harmonic acoustics. *Comput Meth Appl* 2006;195:1594–607.
- [4] Bathe KJ. The finite element method. In: Wah B, editor. *Encyclopedia Comput Sci Eng*. J. Wiley and Sons; 2009. p. 1253–64.
- [5] Lee R, Cangellaris AC. A study of discretization error in the finite-element approximation of wave solutions. *IEEE T Antenn Propag* 1992;40:542–9.
- [6] Guddati MN, Yue B. Modified integration rules for reducing dispersion error in finite element methods. *Comput Meth Appl Mech Eng* 2004;193:275–87.
- [7] Ihlenburg F, Babuška I. Finite element solution of the Helmholtz-equation with high wave-number.1. The h-version of the FEM. *Comput Math Appl* 1995;30:9–37.
- [8] Ihlenburg F, Babuška I. Finite element solution of the Helmholtz equation with high wave number.2. The h-p version of the FEM. *SIAM J Numer Anal* 1997;34:51–58.
- [9] Deraemaeker A, Babuška I, Bouillard P. Dispersion and pollution of the FEM solution for the Helmholtz equation in one, two and three dimensions. *Int J Numer Meth Eng* 1999;46:471–99.
- [10] Babuška IM, Sauter SA. Is the pollution effect of the FEM avoidable for the Helmholtz equation considering high wave numbers? *SIAM Rev* 2000;42:451–84.
- [11] Bathe KJ, Wilson EL. Stability and accuracy analysis of direct integration methods. *Earthquake Eng Struct* 1973;1:283–91.
- [12] Chin RCY. Dispersion and Gibbs phenomenon associated with difference approximations to initial boundary-value problems for hyperbolic equations. *J Comput Phys* 1975;18:233–47.
- [13] Marfurt KJ. Accuracy of finite-difference and finite-element modeling of the scalar and elastic wave-equations. *Geophysics* 1984;49:533–49.
- [14] Wang YC, Murti V, Valliappan S. Assessment of the accuracy of the Newmark method in transient analysis of wave-propagation problems. *Earthquake Eng Struct* 1992;21:987–1004.
- [15] Zingg DW, Lomax H, Jurgens H. High-accuracy finite-difference schemes for linear wave propagation. *SIAM J Sci Comput* 1996;17:328–46.
- [16] Lee JF, Lee R, Cangellaris A. Time-domain finite-element methods. *IEEE T Antenn Propag* 1997;45:430–42.
- [17] Juntunen JS, Tsiaboukis TD. Reduction of numerical dispersion in FDTD method through artificial anisotropy. *IEEE T Microw Theory* 2000;48:582–8.
- [18] Cherukuri HP. Dispersion analysis of numerical approximations to plane wave motions in an isotropic elastic solid. *Comput Mech* 2000;25:317–28.
- [19] Krenk S. Dispersion-corrected explicit integration of the wave equation. *Comput Meth Appl Mech Eng* 2001;191:975–87.
- [20] Atkinson JH, Westerink JJ, Luettich RA. Two-dimensional dispersion analyses of finite element approximations to the shallow water equations. *Int J Numer Meth Fl* 2004;45:715–49.
- [21] Yue B, Guddati MN. Dispersion-reducing finite elements for transient acoustics. *J Acoust Soc Am* 2005;118:2132–41.
- [22] Gabriel D, Plešek J, Kolman R, Valeš F. Dispersion of elastic waves in the contact-impact problem of a long cylinder. *J Comput Appl Math* 2010;234:1930–6.
- [23] Idesman AV, Schmidt M, Foley JR. Accurate finite element modeling of linear elastodynamics problems with the reduced dispersion error. *Comput Mech* 2011;47:555–72.
- [24] Melenk JM, Babuška I. The partition of unity finite element method: Basic theory and applications. *Comput Meth Appl Mech Eng* 1996;139:289–314.
- [25] Laghrouche O, Bettess P, Astley RJ. Modelling of short wave diffraction problems using approximating systems of plane waves. *Int J Numer Meth Eng* 2002;54:1501–33.
- [26] El Kacimi A, Laghrouche O. Numerical modelling of elastic wave scattering in frequency domain by the partition of unity finite element method. *Int J Numer Meth Eng* 2009;77:1646–69.
- [27] El Kacimi A, Laghrouche O. Improvement of PUFEM for the numerical solution of high-frequency elastic wave scattering on unstructured triangular mesh grids. *Int J Numer Meth Eng* 2010;84:330–50.
- [28] Gottlieb D, Orszag SA. Numerical analysis of spectral methods: Theory and applications. Capital City Press; 1993.
- [29] Patera AT. A spectral element method for fluid-dynamics-laminar-flow in a channel expansion. *J Comput Phys* 1984;54:468–88.
- [30] Komatitsch D, Vilotte JP. The spectral element method: An efficient tool to simulate the seismic response of 2D and 3D geological structures. *B Seismol Soc Am* 1998;88:368–92.
- [31] Komatitsch D, Vilotte JP, Vai R, Castillo-Covarrubias JM, Sanchez-Sesma FJ. The spectral element method for elastic wave equations-application to 2-D and 3-D seismic problems. *Int J Numer Meth Eng* 1999;45:1139–64.
- [32] Komatitsch D, Barnes C, Tromp J. Simulation of anisotropic wave propagation based upon a spectral element method. *Geophysics* 2000;65:1251–60.
- [33] Lee U, Kim J, Leung AYT. The spectral element method in structural dynamics. *Shock Vib* 2000;32:451–65.
- [34] Karniadakis GE, Sherwin SJ. Spectral/hp element methods for computational fluid dynamics. Oxford University Press; 2005.
- [35] Stupazzini M, Zambelli C, Massidda L, Paolucci R, Maggio F, Prisco C. The spectral element method as an effective tool for solving large scale dynamic soil-structure interaction problems. In: *Proceedings of the eighth U.S. National Conference on Earthquake Engineering*, 2006.
- [36] Seriani G, Oliveira SP. Dispersion analysis of spectral element methods for elastic wave propagation. *Wave Motion* 2008;45:729–44.
- [37] Zhong WX, Howson WP, Williams FW. Precise solutions for surface wave propagation in stratified material. *J Vib Acoust* 2001;123:198–204.
- [38] Cho J, Lee U. An FFT-based spectral analysis method for linear discrete dynamic systems with non-proportional damping. *Shock Vib* 2006;13:595–606.
- [39] Chakraborty A, Gopalakrishnan S. A spectral finite element model for wave propagation analysis in laminated composite plate. *J Vib Acoust* 2006;128:477–88.
- [40] Gopalakrishnan S, Chakraborty A, Roy Mahapatra D. Spectral finite element method. Springer-Verlag; 2008.
- [41] Cockburn B, Karniadakis G, Shu CW. Discontinuous Galerkin methods: Theory, computation, and applications. Springer; 2000.
- [42] Arnold DN, Brezzi F, Cockburn B, Marini LD. Unified analysis of discontinuous Galerkin methods for elliptic problems. *SIAM J Numer Anal* 2002;39:1749–79.
- [43] Brezzi F, Cockburn B, Marini LD, Suli E. Stabilization mechanisms in discontinuous Galerkin finite element methods. *Comput Meth Appl Mech Eng* 2006;195:3293–310.
- [44] Massimi P, Tezaur R, Farhat C. A discontinuous enrichment method for three-dimensional multiscale harmonic wave propagation problems in multi-fluid and fluid-solid media. *Int J Numer Meth Eng* 2008;76:400–25.
- [45] Petersen S, Farhat C, Tezaur R. A space-time discontinuous Galerkin method for the solution of the wave equation in the time domain. *Int J Numer Meth Eng* 2009;78:275–95.
- [46] Bathe KJ, Almeida CA. A simple and effective pipe elbow element—linear analysis. *ASME J Appl Mech* 1980;47:93–100.
- [47] Bathe KJ, Almeida CA, Ho LW. A simple and effective pipe elbow element—some non-linear capabilities. *Comput Struct* 1983;17:659–67.
- [48] Bathe KJ, Chaudhary A. On the displacement formulation of torsion of shafts with rectangular cross-sections. *Int J Numer Meth Eng* 1982;18:1565–8.
- [49] Bathe KJ, Zhang H. A flow-condition-based interpolation finite element procedure for incompressible fluid flows. *Comput Struct* 2002;80:1267–77.
- [50] Banijamali B, Bathe KJ. The CIP method embedded in finite element discretizations of incompressible fluid flows. *Int J Numer Meth Eng* 2007;71:66–80.
- [51] Strouboulis T, Copps K, Babuska I. The generalized finite element method: An example of its implementation and illustration of its performance. *Int J Numer Meth Eng* 2000;47:1401–17.
- [52] Fries TP, Belytschko T. The extended/generalized finite element method: An overview of the method and its applications. *Int J Numer Meth Eng* 2010;84:253–304.
- [53] Lee NS, Bathe KJ. Effects of element distortions on the performance of isoparametric elements. *Int J Numer Meth Eng* 1993;36:3553–76.
- [54] Bathe KJ. Conserving energy and momentum in nonlinear dynamics: A simple implicit time integration scheme. *Comput Struct* 2007;85:437–45.
- [55] Christon MA. The influence of the mass matrix on the dispersive nature of the semi-discrete, second-order wave equation. *Comput Meth Appl Mech Eng* 1999;173:147–66.
- [56] Achenbach JD. Wave propagation in elastic solids. North-Holland; 1973.
- [57] Aki K, Richards PG. Quantitative seismology. University Science Books; 2002.
- [58] Lai CG, Wilmanski K. Surface waves in geomechanics: Direct and inverse modelling for soils and rocks. Springer; 2005.
- [59] Kausel E. Fundamental solutions in elastodynamics: A compendium. Cambridge University Press; 2006.
- [60] Bermudez A, Hervella-Nieto L, Prieto A, Rodriguez R. An optimal perfectly matched layer with unbounded absorbing function for time-harmonic acoustic scattering problems. *J Comput Phys* 2007;223:469–88.
- [61] Buecalem ML, Bathe KJ. The mechanics of solids and structures - hierarchical modeling and the finite element solution. Springer; 2011.
- [62] Grätsch T, Bathe KJ. A posteriori error estimation techniques in practical finite element analysis. *Comput Struct* 2005;83:235–65.
- [63] Bathe KJ, Brezzi F, Cho SW. The MITC7 and MITC9 plate bending elements. *Comput Struct* 1989;32:797–814.
- [64] Chapelle D, Bathe KJ. The finite element analysis of shells - fundamentals. Springer; 2011.
- [65] Bathe KJ, Lee PS. Measuring the convergence behavior of shell analysis schemes. *Comput Struct* 2011;89:285–301.
- [66] Bathe KJ. The inf-sup condition and its evaluation for mixed finite element methods. *Comput Struct* 2001;79:243–52.
- [67] Bathe KJ, Zhang H, Yan Y. The solution of Maxwell's equations in multiphysics, in preparation.
- [68] Kazanci Z, Bathe KJ. Crushing and crashing of tubes with implicit time integration. *Int J Impact Eng* 2012;42:80–8.